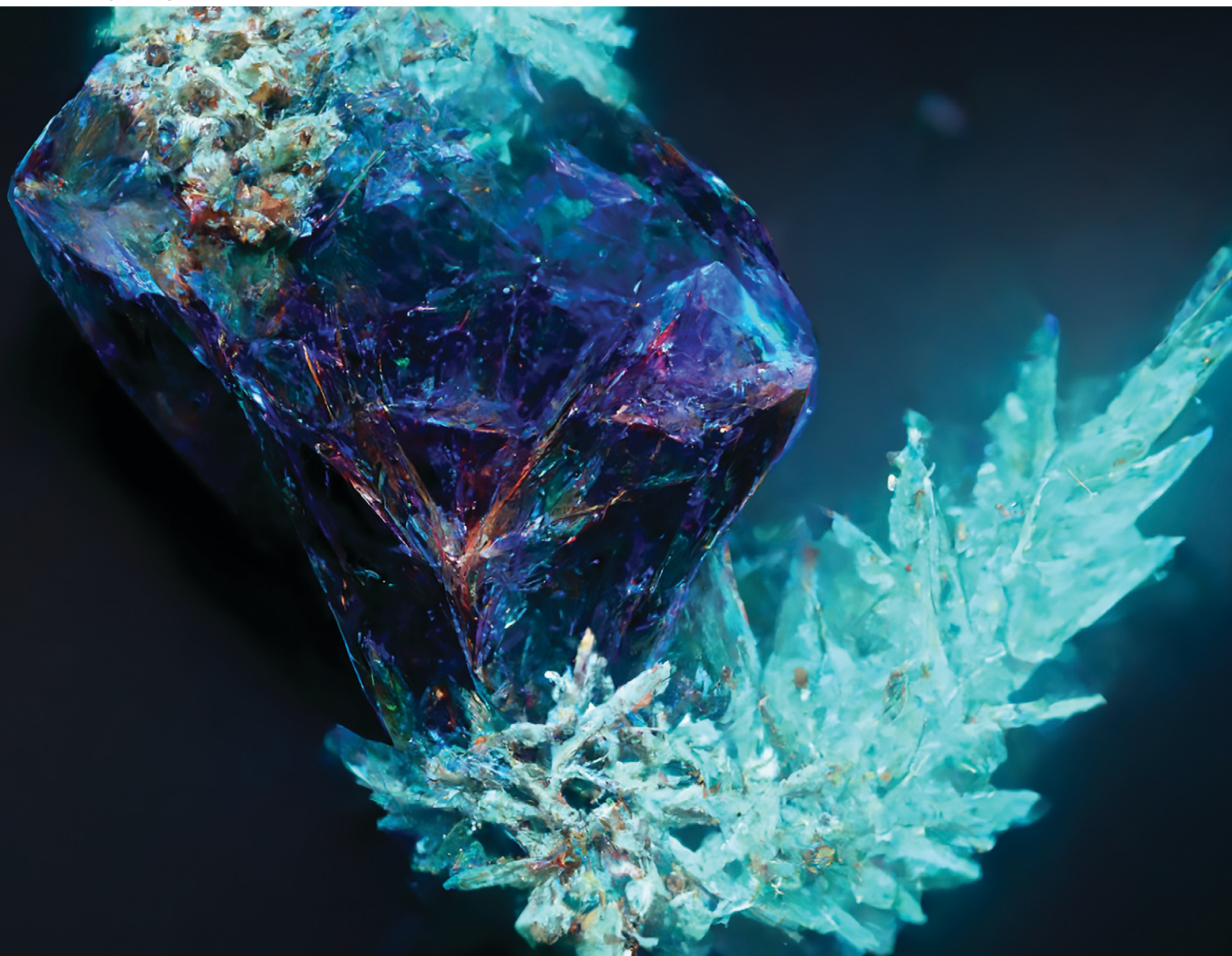


CrystEngComm

rsc.li/crystengcomm



ISSN 1466-8033

PAPER

Artur Mirocki *et al.*

Exploring the molecular landscape of multicomponent
crystals formed by naproxen drug and acridines



Cite this: *CrystEngComm*, 2022, 24, 6839

Exploring the molecular landscape of multicomponent crystals formed by naproxen drug and acridines†

Artur Mirocki, ^a Mattia Lopresti, ^b Luca Palin, ^{bc} Eleonora Conterosito, ^b Artur Sikorski ^a and Marco Milanesio ^{*b}

The cocrystallization of active pharmaceutical ingredient naproxen with some acridines (acridine, 9-aminoacridine, 6,9-diamino-2-ethoxyacridine) has been explored and the conditions under which the crystallization can be carried out have been investigated. While the crystallization of acridine-based molecular crystals was widely studied under solution conditions, solvent-free and/or mechanochemical method potentialities are still unknown. To fill this gap, the cocrystallization of naproxen with the above-mentioned acridines was attempted using different approaches, e.g., by heat treatment of the dry mechanical mixture and by liquid-assisted grinding (LAG), as alternatives to the traditional precipitation by a proper solution. In the first case, the reaction is driven under dry conditions by the temperature and gave no results independently of the temperature used, below or above the melting point of the reactants. In the second case, the reaction is driven by the mechanical action of grinding assisted by a few drops of solvent to facilitate and improve the reaction. This screening allowed obtaining three new molecular crystals for naproxen coupled to acridine and a mono-aminoacridine and solved by single-crystal and powder X-ray diffraction (PXRD). Two host-guest structures were obtained by solution crystallization, while a layered structure was obtained under LAG conditions. Interconversion between molecular crystals formed by the same chemical species was hindered once a molecular crystal was obtained by a specific technique. Hirshfeld and energy framework calculations confirmed the remarkable structural differences between **1 α** and **1 β** packing and suggested that **1 β** is kinetically more stable. Variable-temperature PXRD, DSC and TGA were used to explore the stability of the compounds. 6,9-Diamino-2-ethoxyacridine proved to be too polar and/or too bulky to form crystals with naproxen regardless of the preparation method and the different stoichiometric ratios used. It is noteworthy that LAG allowed the preparation of the naproxen/acridine molecular crystal with a yield higher than 99% under almost solvent-free conditions. DSC indicated the formation of a eutectic between naproxen and acridine, with the possibility of recrystallizing the 1:1 complex also from the melt solution.

Received 30th June 2022,
Accepted 4th September 2022

DOI: 10.1039/d2ce00890d

rsc.li/crystengcomm

1. Introduction

Crystal engineering is an intensively developing field, and one of its main assumptions is to identify and understand intermolecular interactions in crystals.^{1–4} It allows the design and preparation of new materials based on a repeatable

structural motif (synthons) arising through intermolecular interactions between different functional groups in the molecules. The knowledge on how the synthons assemble is fundamental to obtain multicomponent crystals with the desired, predictable structure as well as the expected properties. However, a change of the stoichiometry of the cocrystals and an increase in the number of functional groups in the molecules used may lead to unexpected changes in the structural landscape of multicomponent crystals. All these issues are even more important when the synthons are active pharmaceutical ingredients (APIs). In this case, small changes in the molecular formula and/or in the crystal packing might affect the solubility, bioavailability and other properties related to their biological activity. The formulation of APIs is thus one among the key steps when transforming a bioactive molecule into a drug. A common

^a Faculty of Chemistry of the University of Gdansk, ul. Wita Stwosza 63, 80-308 Gdansk, Poland

^b Università del Piemonte Orientale, Dipartimento di Scienze e Innovazione Tecnologica, Viale T. Michel 11, 15121 Alessandria, Italy.
E-mail: marco.milanesio@uniupo.it

^c Nova Res s.r.l., Via D. Bello 3, 28100 Novara, Italy

† Electronic supplementary information (ESI) available. CCDC 2168756, 2168757 and 2169121. For ESI and crystallographic data in CIF or other electronic format see DOI: <https://doi.org/10.1039/d2ce00890d>



package.³⁷ The structures were solved with direct methods that carried out refinements by full-matrix least-squares on F^2 using the SHELXL-2017/1 program.³⁷ All H atoms bound to O/N atoms were located on a difference Fourier map and refined freely with $U_{\text{iso}}(\text{H}) = 1.5/1.2U_{\text{eq}}(\text{O/N})$. All H atoms bound to C atoms were placed geometrically and refined using a riding model with $d_{(\text{C-H})} = 0.93\text{--}0.98 \text{ \AA}$ and $U_{\text{iso}}(\text{H}) = 1.2U_{\text{eq}}(\text{C})$ ($d_{(\text{C-H})} = 0.96 \text{ \AA}$ and $U_{\text{iso}}(\text{H}) = 1.5U_{\text{eq}}(\text{C})$ for the methyl groups). All interactions were calculated using the PLATON program.³⁸ The following programs were used to prepare the molecular graphics: ORTEP II,³⁹ PLUTO-78,⁴⁰ and Mercury.⁴¹ Full crystallographic details of the structures reported in this paper have been deposited with the Cambridge Crystallographic Data Centre (deposition no. CCDC 2168756, CCDC 2169121 and CCDC 2168757 for **1 α** , **1 β** and **2 α** , respectively).

2.3. Powder X-ray diffraction

PXRD analysis was performed on a Bruker D8 Advance diffractometer with a Lynx-Eye XE-T detector and Cu K_{α} ($\lambda = 1.5418 \text{ \AA}$) radiation (Table 2). The goniometer radius is 280 mm. The tube was set at 40 mA current and 40 kV electric potential. The instrument was at first used as an analytical qualitative tool to evaluate if the reaction occurred and to assess the purity of the product. Then it was used to understand if the single-crystal structure is representative of the complete batch or if just the mechanical mixture of the reactant was present after synthesis attempts and thus to identify the best (or not) preparation procedures. When enough sample was available, an auto-sampler with nine positions, rotating sample holders and an air scatter knife was used. On both the primary and secondary optics, Soller slits of 2.5° opening were positioned. The patterns were collected in Bragg–Brentano geometry from 3° to 70° 2θ with a step size of 0.01° and exposure time of 0.05 s; automatic divergence slits were set to obtain constant sample illumination of 17 mm. The dry synthesis was carried out in sealed 0.7 mm glass capillaries placed in an oven and directly used for the measurements (0.6 mm planar slit used with a step size of 0.0204° and exposure time of 0.5 s). The capillary setup was also utilized to obtain an optimal angle resolution with a FWHM of about 0.01° suitable for indexing of **1 β** , obtained only by LAG in polycrystalline form. The measurement was carried out using a planar 0.6 mm slit, a step-size of 0.005° and exposure time of 5 s, and this 18 hour measurement resulted in a **1 β** crystal structure suitable for solving and refinement. Structure solution was carried out by simulated annealing in real space by EXPO⁴² from capillary data, while final structure refinement was carried out by Topas Academic^{43,44} on capillary and flat sample data. *In situ* X-ray diffraction study of the LAG procedure was applied to single crystals of **1 α** using a focusing optic (Goebel mirror with 1 mm focusing hole) after positioning the sample by the xyz stage. A variable-temperature powder X-ray diffraction experiment was performed by installing a Linkam THMS600

variable-temperature stage within the motorized xyz stage (UMC compact stage) of a Bruker D8 Advance diffractometer to obtain a PXRD setup able to manage liquids. The standard Linkam cover was removed to allow X-rays to reach the sample and a Kapton foil was used to avoid evaporation. The sample was positioned in a 10 mm diameter sample holder for liquids and patterns were collected on a same length illuminated area every 40 seconds. PXRD patterns were measured in the 2θ range of $8\text{--}31^{\circ}$ with an increment of 0.025° and a step time of 0.03 s. A USB microscope was used to obtain the image of the sample before each PXRD measurement to check if the sample appears liquid or solid.

2.4. Thermal analysis

DSC was carried out using a TA Q200 and a METTLER TOLEDO DSC 3 analyzer. For both instruments a closed aluminium pan was used with a ramp rate of $5 \text{ }^{\circ}\text{C min}^{-1}$. TGA was carried out using a TA Q600 STD analyzer and an alumina crucible at a ramp rate of $10 \text{ }^{\circ}\text{C min}^{-1}$ in an oxidizing environment.

2.5. Hirshfeld surfaces and energy framework calculations

Hirshfeld surfaces with electron density, fingerprint plots and energy frameworks were calculated using CrystalExplorer 17.5 (ref. 45) and analysed for the three solved structures. Hirshfeld surfaces were calculated with a high-resolution setting. The wavefunctions for each molecule and pairwise interaction for the calculation of energy frameworks were calculated using Tonto with the B3LYP DFT method by employing the 6-31G(d,p) basis set, as implemented in CrystalExplorer. The scale for the tube size employed for energy framework pictures is 80 and the cut-off value for energies was set to 0 kJ mol^{-1} . Interaction energies between each independent molecule and its neighbours were calculated and from this the sum of the lattice energy for each unique molecule was obtained as one-half the product of the number of symmetry equivalent molecules in the cluster and the total energy.⁴⁶

3. Results and discussion

3.1. Crystal structure solution

The preparation of the three possible couples between naproxen and the three acridines in Scheme 1 was carried out by solution, LAG and a thermal dry procedure and the results are summarized in Table 1. A cocrystal of naproxen with acridine (2:3 stoichiometry) (**1 α**) and a monohydrate salt cocrystal of naproxen with 9-aminoacridine (2:1 stoichiometry) (**2 α**) were obtained through the reactions carried out in solution. Conversely, powdered cocrystals of naproxen with acridine (1:1 stoichiometry) (**1 β**) were obtained by the reactions carried out under LAG conditions, as reported in Table 1. These forms are those expected from the $\text{p}K_{\text{a}}$ difference of the reactants, which is larger than 3 only for the **2 α** couple.



Table 1 Summary of the applied preparation methods and obtained molecular crystals

| API | Coformer | Compound | Solution | Dry | LAG |
|----------|------------------------------|----------|---------------------------------|---------------------------------|---------------------------------|
| Naproxen | Acridine | 1 | Single crystals 1α | Mechanical mixture of reactants | Powder 1β |
| | 9-Aminoacridine | 2 | Single crystals 2α | | Mechanical mixture of reactants |
| | 6,9-Diamino-2-ethoxyacridine | — | Mechanical mixture of reactants | | Mechanical mixture of reactants |

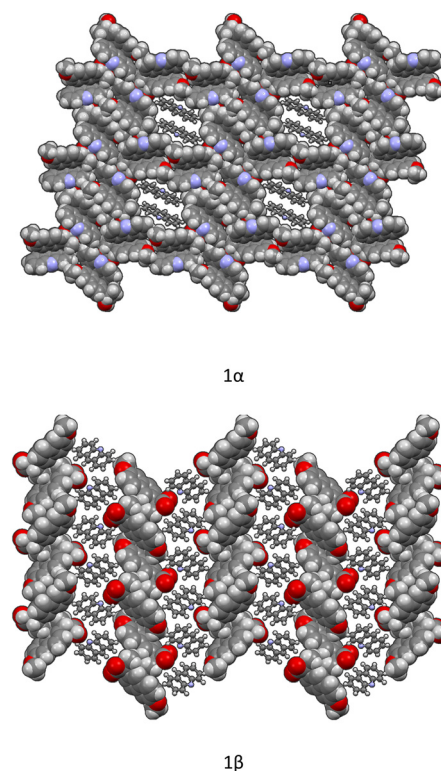
Table 2 Crystal data and structure refinement for **1α**, **2α** and **1β**

| Compound | 1α (SX) | 2α (SX) | 1β (PXR) |
|--|---|---|---|
| Chemical formula | C ₆₇ H ₅₅ N ₃ O ₆ | C ₄₁ H ₄₀ N ₂ O ₇ | C ₂₇ H ₂₃ NO ₃ |
| Formula weight/g mol ⁻¹ | 998.14 | 672.75 | 409.48 |
| Crystal system | Monoclinic | Monoclinic | Orthorhombic |
| Space group | <i>P</i> 2 ₁ | <i>P</i> 2 ₁ | <i>P</i> 2 ₁ 2 ₁ 2 ₁ |
| <i>a</i> /Å | 17.3435(14) | 10.0768(11) | 12.6466(4) |
| <i>b</i> /Å | 5.9437(6) | 6.2918(5) | 29.6246(12) |
| <i>c</i> /Å | 25.672(2) | 27.347(3) | 5.63596(19) |
| <i>α</i> /° | 90 | 90 | 90 |
| <i>β</i> /° | 101.975(9) | 98.004(11) | 90 |
| <i>γ</i> /° | 90 | 90 | 90 |
| <i>V</i> /Å ³ | 2588.8(4) | 1717.0(3) | 2111.52 |
| <i>ρ</i> _{calc} /g cm ⁻³ | 1.280 | 1.301 | 1.288 |
| Final <i>R</i> ₁ value | 0.0585 | 0.0677 | <i>R</i> _p = 2.043 |
| Final <i>wR</i> ₂ value | 0.0927 | 0.0843 | <i>R</i> _{wp} = 2.635 |
| CCDC number | 2168756 | 2168757 | 2169121 |

Crystallization from solution produced single crystals by coupling naproxen to acridine and 9-aminoacridine, while no results were obtained for naproxen/6,9-diamino-2-ethoxyacridine. Single-crystal X-ray diffraction measurements show that compound **1α** crystallizes from solution in the monoclinic *P*2₁ space group as a cocrystal with two naproxen and three acridine molecules in the asymmetric unit (Fig. S1† and Table 2). Compound **2α** crystallizes in the monoclinic *P*2₁ space group as a monohydrate salt cocrystal with one naproxen molecule and anion, one 9-aminoacridinium cation, and one water molecule in the asymmetric unit (Fig. S2† and Table 2). Both **1α** (Fig. 1, top) and **2α** (Fig. 2) show a host-guest-like packing. LAG and dry thermal synthesis were thus performed as described in the Experimental section for all the three acridines and the results are summarized in Table 1. While dry synthesis was unsuccessful in all cases, the LAG approach allowed obtaining a cocrystal of naproxen with acridine (1:1 stoichiometry) (**1β**). In fact, analysis by powder X-ray diffraction (Fig. 3) confirmed that the patterns of the products obtained by LAG (the reactant with a 3:2 naproxen/acridine ratio as in **1α**) did not coincide with those obtained by solution or with the patterns corresponding to the mechanical mixture of the reagents. The new molecular cocrystal appeared with a residual amount of acridine reactant. The LAG procedure was thus repeated with a 1:1 naproxen/acridine reactant ratio and pure **1β** was obtained, within the sensibility limitation of powder diffraction (Table 2). For further confirmation, the reagents were also subjected to the LAG procedure individually to verify that the

products obtained were not mechanical mixtures of molecular crystals of the reagents alone due to the LAG process. In Fig. 3, the PXR patterns of both molecular crystals **1α** and **1β** of naproxen/acridine cocrystals confirm that their crystal structures are different. To obtain a PXR pattern suitable for structure solution, a capillary was filled, and a long measurement was carried out to obtain a good resolution. This pattern was used to index and obtain a cell. Then, the structure solution was carried out using the same data based on the available diffraction data; the obtained crystal structure is presented in Fig. 1, bottom. It is worth noting that the product is pure, within the sensitivity limitation of PXR, as indicated by the Rietveld refinement reported in Fig. 3.

In both molecular crystals **1α** and **1β**, the packing is due to two different driving forces: in the case of the 2:3 molecular crystal **1α**, intermolecular COOH_(naproxen)⋯N_(acridine) and OH_(naproxen)⋯N_(acridine) hydrogen bonds and C-H_(naproxen/acridine)⋯π_(naproxen/acridine) interactions prevail

**Fig. 1** Crystal packing of **1α** and **1β**.

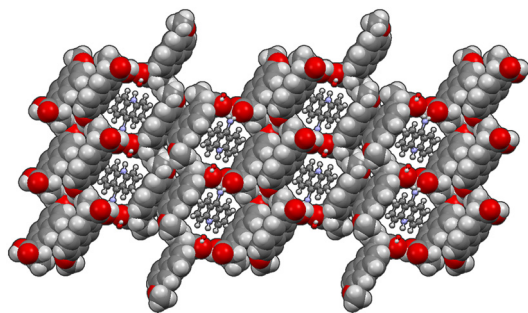


Fig. 2 Crystal packing of 2α .

(Tables S3 and S4[†]), while in the case of the 1:1 ratio molecular crystal 1β , there is an overall stabilization of the structure given by π -stacking and intermolecular and the above-mentioned O–H \cdots N hydrogen bonds. In detail, each naproxen is bonded by one H-bond and CH \cdots O interactions

to two different acridine molecules (Table S2[†]). A T-like interaction and a parallel π - π interaction connect adjacent acridine layers as detailed in Table S3.[†] Several CH \cdots C longer contacts (mainly involving naproxen methyl groups) complete the packing. Consequently, in the crystal of 1α , hydrogen-bonded pairs of naproxen and acridine molecules formed the 3D network, with voids filled by the non-hydrogen-bonded acridine molecules. Of course, the host-guest structure cannot be considered a MOF-like compound since the guest cannot be removed without destroying its crystal structure. Conversely, in 1β , π -stacked columns of acridine molecules and the layered association of naproxen molecules can be observed as previously observed in the molecular crystals of naproxen with proline (1:1) (described by authors as type II).²⁰ A weak CH \cdots O and a strong OH \cdots N hydrogen bond interaction connect the layers of naproxen with those of acridine. This packing was obtained after carefully checking all the possibilities in placing the acridine molecule (that can

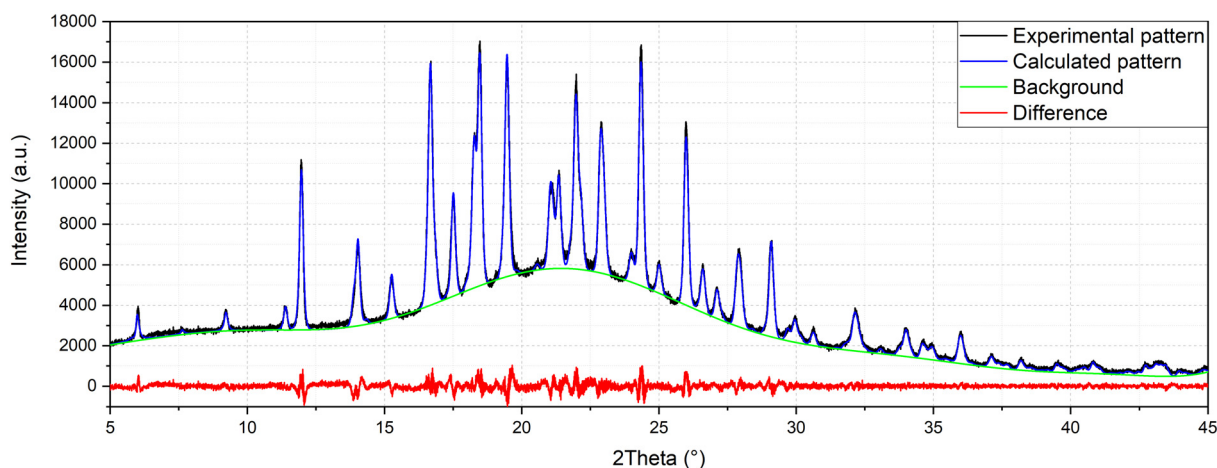
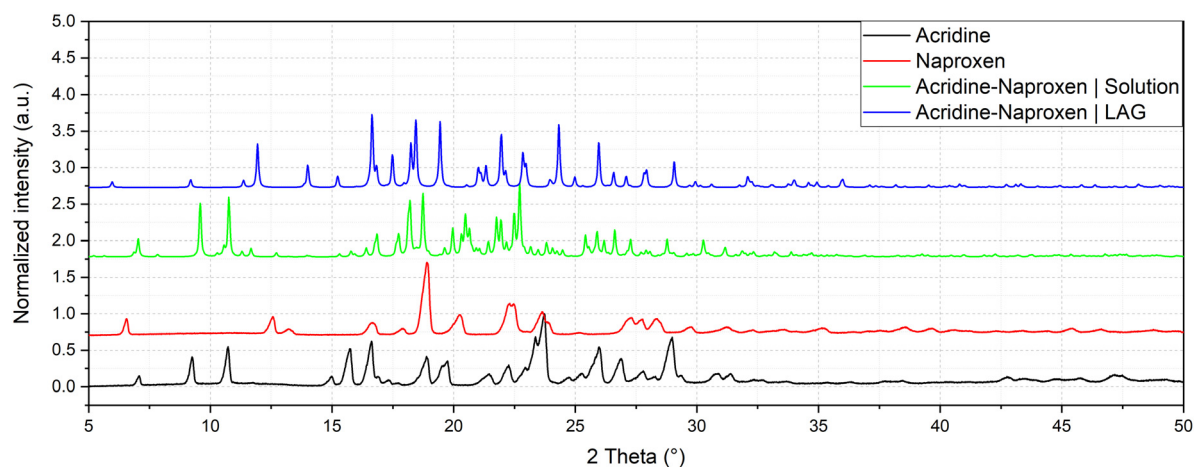


Fig. 3 Comparison of powder patterns of 1α and 1β and refinement of crystal structure solved by powder diffraction of 1β ($R_p = 2.043$, $R_{wp} = 2.635$).



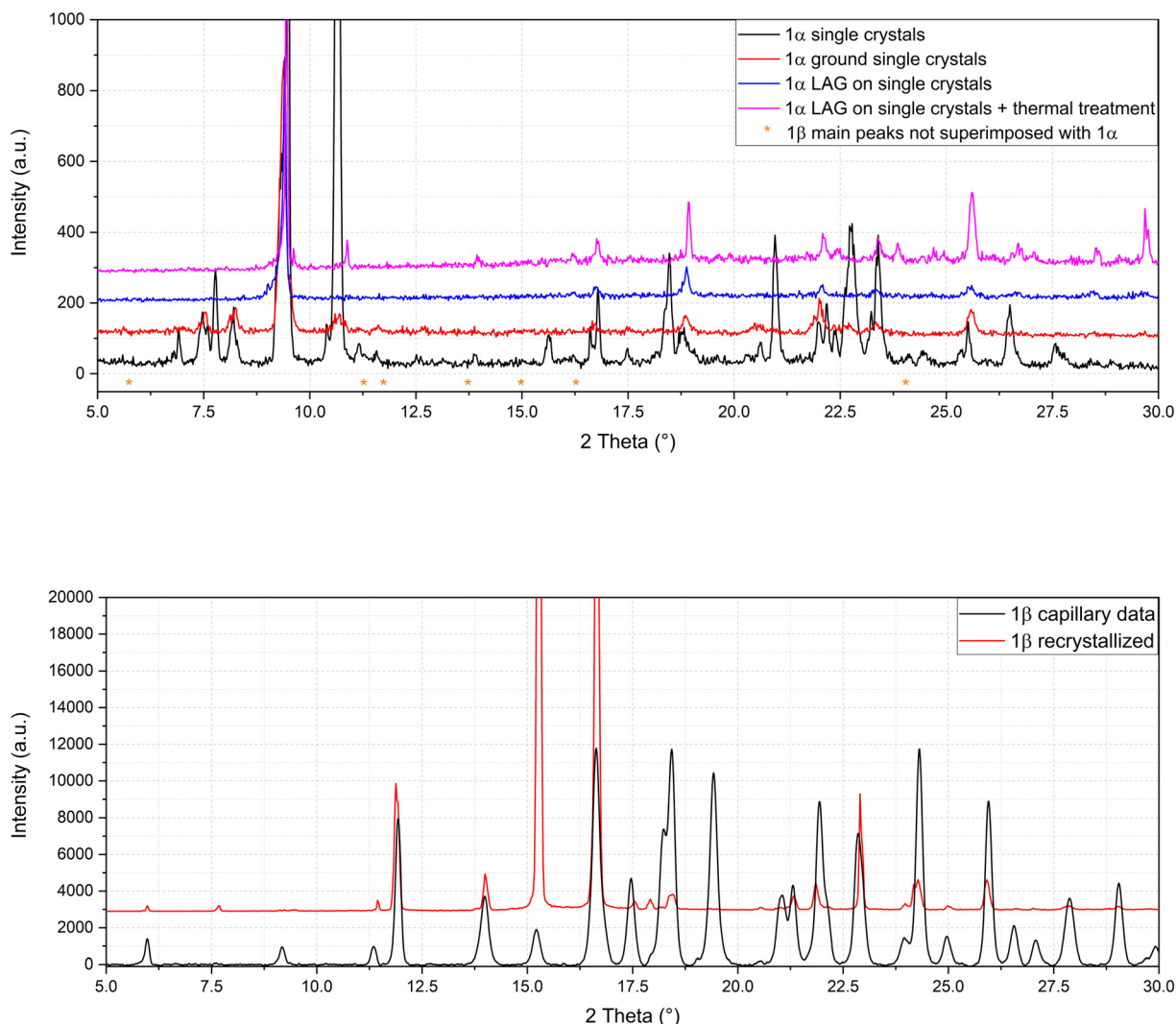


Fig. 5 Refinement of **1α** after LAG (top) and solution crystallization of **1β** after full dissolution (bottom).

can be readily seen between Mol_1 and Mol_2_n and a slightly shorter one between Mol_4_a and Mol_5_n. Mol_1_a and Mol_2_n also share an O \cdots H interaction, while Mol_5_n has an O \cdots H interaction with a symmetry equivalent molecule. The more symmetrical plot of Mol_3_a evidences a predominance of interactions with symmetry equivalent molecules. There is no evidence by looking at both the Hirshfeld surfaces and fingerprint plots of π - π interactions (C \cdots C).

The most important interactions in **1β** shown by Hirshfeld surface analysis (Fig. 7) are the OH \cdots N hydrogen bond between acridine and naproxen, separated by a short contact distance (2.08 Å) clearly evidenced by plotting d -norm on the surfaces (Fig. 7, bottom), and the presence of π - π stacking between acridine molecules. The fingerprint plots are shown in the top part of Fig. 7 for acridine (Mol_1_a) and naproxen (Mol_2_n). The fingerprint plot features are labelled according to the interaction; the first atom is the one inside the surface. The hydrogen bond is clearly shown by a spike in both plots, indicating a short-range contact between the N atom in acridine and the OH group in naproxen, while the

π - π interaction (C \cdots C) is found at longer distances and occurs between acridine molecules. This feature is clearly visible only in the acridine plot, represented by a green symmetrical spot at 1.8 Å on both axes, indicating a contact distance of about 3.6 Å.

From the analysis of the Hirshfeld surfaces and fingerprint plots of **2α** (Fig. S9 and S10, respectively, in the ESI †) it appears that the shorter interactions are hydrogen bonds, the one between the water molecule and Mol_1_a (9-aminoacridinium). Other hydrogen bonds are formed between the naproxen moieties and water, while N \cdots H interactions are long range and can be seen in the fingerprint plot only after filtering (Fig. S10, ‡ bottom). It is also worth noting the formation of π - π interactions between 9-acridinium molecules (Mol_1_a) evidenced by a green spot in the fingerprint plot as in **1β**.

The energy frameworks were also calculated for all structures. In Fig. 8 the energy frameworks for the coulombic interactions are reported showing that in **1α** the stronger interactions (thicker tubes in the picture) form a crossed



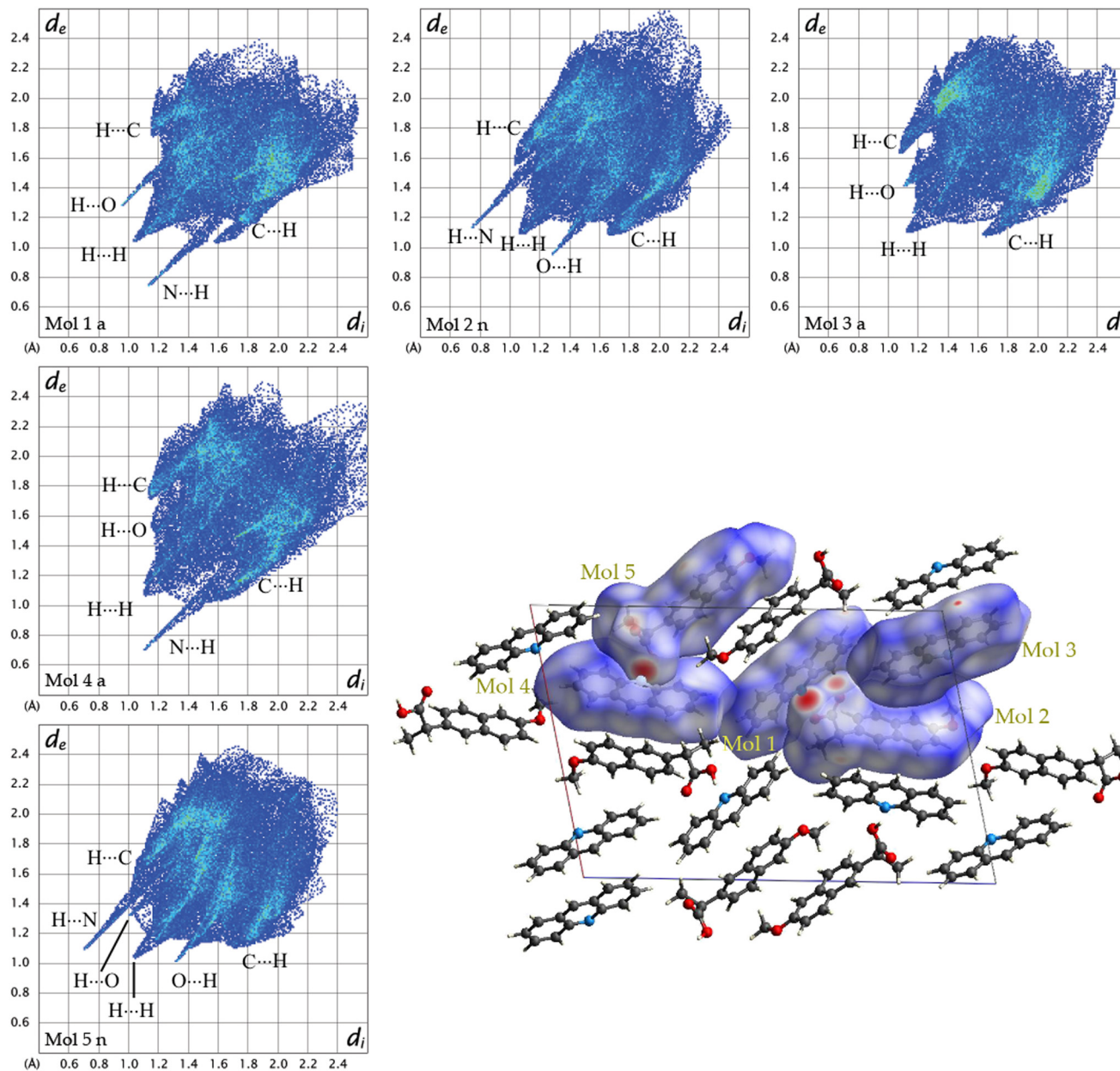


Fig. 6 Fingerprint plots for each symmetry-independent molecule in 1α and crystal structure model of 1α viewed along the b -axis showing Hirshfeld surfaces with d -norm plotted.

pattern, while in 1β the interactions are almost parallel, forming a layered structure. Remarkable differences can be seen also in the dispersion interactions, forming a honeycomb-like motif in 1α viewed along the b -axis, while a square motif is observed for 1β . In this structure, along the b -axis the packing is stabilised mainly by coulombic forces, while dispersion forces are stronger in the perpendicular directions. Therefore, the layers are kept together by π - π interactions while the interaction between the layers is polar (*i.e.* hydrogen bonds).

From the calculation of pairwise interactions, the lattice energy was calculated for each independent molecule. For structure 1β the sum of energies for the acridine molecule

was found to be about -90 kJ mol^{-1} , while for naproxen it was -108 kJ mol^{-1} . For structure 1α the energies for the acridine molecules resulted to be -100 , -82 and -97 kJ mol^{-1} for Mol_1_a, Mol_3_a and Mol_4_a, respectively (avg. -93 kJ mol^{-1}), while the energies for the naproxen molecules are -122 kJ mol^{-1} for Mol_2_n and -125 kJ mol^{-1} for Mol_5_n (avg. 124 kJ mol^{-1}). Therefore, the average energy for acridine molecules was found to be similar in the two structures, while naproxen appears to be more stable in 1α . These data, keeping in mind the different stoichiometry, allow estimating the lattice energies to be -263 and -198 kJ mol^{-1} for 1α and 1β , respectively, suggesting that 1α is the thermodynamically stable cocrystal.



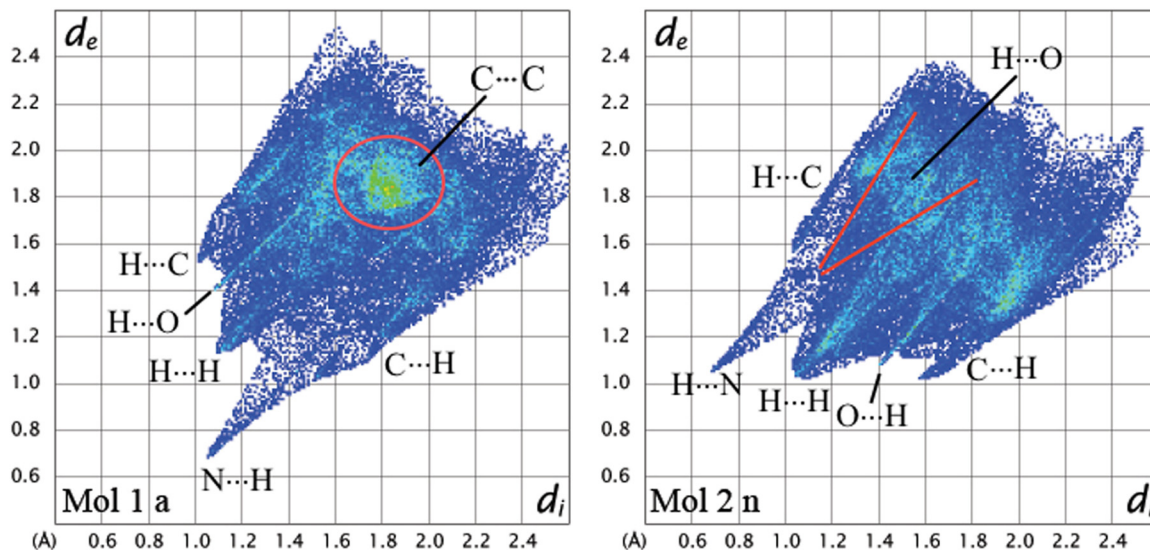


Fig. 7 (Top) Fingerprint plots for acridine (Mol_1_a) and naproxen (Mol_2_n) in **1β** and (bottom) the crystal structure model of **1β** viewed along the *a*-axis showing Hirshfeld surfaces with *d*-norm plotted. Some molecules were omitted for clarity.

The energy frameworks for **2α** are shown in Fig. S11 and S12 in the ESI.† Coulombic energy is shown in Fig. S11;† the attractive interactions are shown in red while repulsive forces are in yellow. The water molecule is involved in the stronger attractive interaction involving the 9-aminoacridinium and naproxen molecules, while repulsion occurs between the aromatic rings and the deprotonated naproxen. The layered motif of the packing is driven by the presence of parallel dispersion forces like in **1β** (see Fig. S12,† view along the *a*-axis). The key role of the water molecule in the crystal packing of **2α** could be the reason why both thermal dry synthesis and LAG were unsuccessful in obtaining a second cocrystal, as in the case of compound **1**.

Finally, to experimentally assess which compound is more stable between **1α** and **1β** and further explore the thermal

behaviour of reactants and products, TGA and DSC analysis of the mechanical mixture of acridine and naproxen and of the cocrystal in their various forms was investigated. TGA was carried out from 40 to 600 °C and the profiles are in Fig. S3.† The maximum of the loss degradation slope profile is at 241 °C for **1α** and at 283 °C for **1β**, clearly suggesting that **1β** is the more stable cocrystal. This indication is apparently contradictory with respect to energy framework calculations, and it could in principle be ascribed to the limitations of this theoretical approach. Another hypothesis could be that the stability of **1β** is due to kinetic reasons. DSC was also measured from 40 to 160 (in the case of acridine when the samples melt at around 105°) or 180 °C (in the case of 9-aminoacridine to reach full melting) and the results are reported in the ESI.† The heating/cooling ramp was cycled to



still present in the melt, and they favour the crystallization instead of the amorphous solidification. In fact, the DSC profile of **1 α** (Fig. S4[†]) shows two broader peaks under heating, but at much lower temperatures, *e.g.*, 50 and 70 °C. This behaviour further confirmed that **1 β** appears to be the more stable compound. From a thermodynamic viewpoint, within the limitation of energy framework calculations, **1 α** seemed more stable than **1 β** , explaining why the LAG treatment of **1 α** is not able to transform this crystal in **1 β** . The unsuccessful conversion of **1 β** to **1 α** , together with the higher temperature signal of **1 β** in TGA and DSC, should be ascribed to kinetic reasons. Conversely, the DSC profile of the mechanical mixture of naproxen and 9-aminoacridine (the reactants of compound **2**) suggests their separate melting (at the expected melting temperature) and a eutectic solidification at 110 °C (Fig. S6[†]) of the two crystalline reactants, confirming a weaker affinity with respect to the acridine/naproxen couple. The PXRD pattern of the analysed sample was collected after the cooling ramp of the DSC (Fig. S7[†]) and, as expected, represents the sum of the two pure phase PXRD profiles, confirming that no reactions occurred, with crystallization of the reactants. Compound **2** can be obtained only by solvent crystallization in the host/guest structure, in analogy to **1 α** and no 1:1 phase was obtained. Finally, these DSC experiments explain the unsuccessful thermal synthesis in the capillary because the crystallization of the melt, independently of the chosen temperature, if the eutectic is reached, gives an amorphous phase.

To summarize, the molecular and structural landscape of compound **1** appears as in Fig. 9. We must conclude that solubilizing **1 β** induces a different result (still **1 β** crystallizes)

with respect to the crystallization after solubilizing the reactants separately (**1 α** crystallizes). Moreover, it must be noted that **1 β** from solution shows a habit (long needles in the optical microscope) different from that of **1 β** obtained from LAG (powder made up of small crystallites) as can be seen by the preferred orientation evident in the pattern of recrystallized **1 β** in Fig. 5, bottom. Except for preferred orientations, this “needle form” showed the same powder pattern of the LAG-obtained sample, confirming the same crystal structure despite the different morphology. This seeding effect of a molecular crystal (**1 β**) prevailing, although it does not appear to be the more thermodynamically stable one, is rare but not new and observed also in famous case studies as those depicted as “the disappearing polymorph” summarized in review some years ago.⁵¹ However, in the present case, the different stoichiometries and solvation degrees of **1 α** and **1 β** can also be other explanations of the impossibility of the mutual interconversion between the two forms.

Concerning the number of molecular crystals obtained using the reactant in Scheme 1, it can be concluded that a clear trend from acridine (two molecular crystals), 9-aminoacridine (one molecular crystal) and 6,9-diamino-2-ethoxyacridine (no cocrystal) is evident. Such results suggest that only compounds with a limited number of polar side chains can be used as cocrystals with naproxen. When the affinity is higher as in the case of **1**, a eutectic is formed upon heating and the 1:1 compound (**1 β**) can be obtained by the LAG method, besides the host/guest compound (**1 α**). When the affinity is smaller, as in the case of **2**, the eutectic is formed only upon cooling of the melt, but the cooling

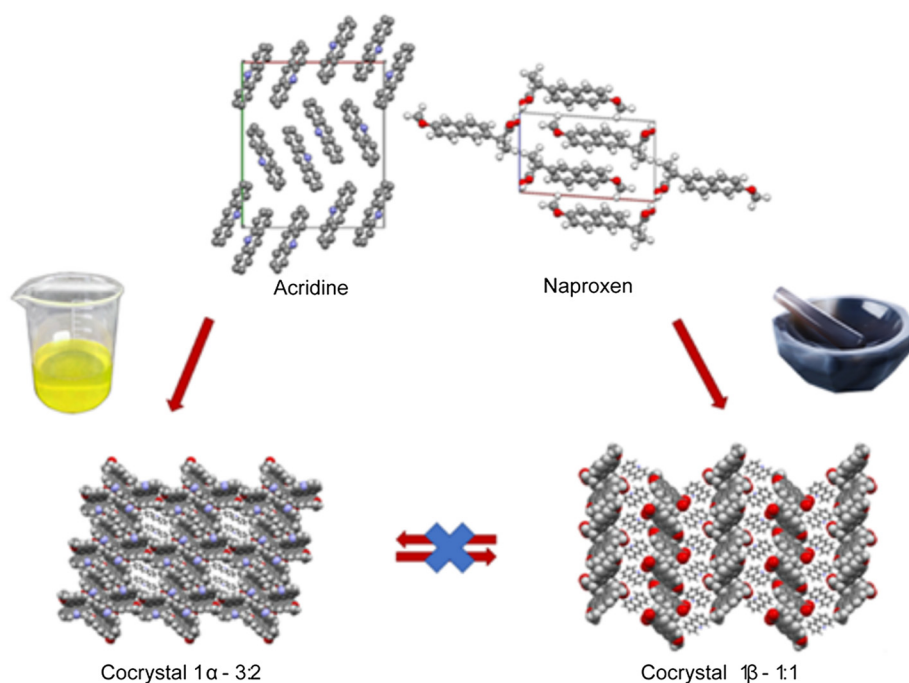


Fig. 9 The molecular landscape of compound **1**.



causes crystallization of the same reactant and the 1:1 layered phase equivalent to **1β** cannot be obtained. Only the host/guest structure (**2α**) can be obtained by solution crystallization. With a bulkier and more polar counterpart (6,9-diamino-2-ethoxyacridine in Scheme 1) no crystallization is observed by any preparation technique. In this case the DSC profile of the mechanical mixture gave contradictory results: a eutectic partial melting is observed at 120 °C (6,9-diamino-2-ethoxyacridine lactate melts at 245°), then a large bump around 140° but a net sharp peak is observed at 175 °C, just some degrees above the naproxen MP (165 °C), followed by amorphous solidification under cooling. These results are not much different from the acridine/naproxen couple, but in this case not one among the three methods used allowed obtaining a crystalline molecular complex despite the affinity observed in the melt state by DSC. The unsuccessful attempt could be due to the use of its common and stable lactate form.

Conclusions

A total of three cocrystals of naproxen with acridines, comprising two cocrystals with a different stoichiometry, were obtained: two through the reaction carried out in solution and one carried out by the LAG procedure. The efficacy of LAG as a means of exploring stoichiometric diversity in molecular cocrystals was confirmed in this study.

Three new crystal structures were obtained, one of them solved by powder diffraction data. The crystallization from solution allowed obtaining solvated 3:2 and 2:1 host-guest structures for **1α** and **2**. Conversely, LAG allowed obtaining a 1:1 layered head-to-tail crystal structure (**1β**) with a yield larger than 99% under almost dry conditions. Surprisingly, the two molecular cocrystals of naproxen with acridine cannot be converted from one to the other, probably because of the different stoichiometry and complex equilibria between reactants and products, governed by contrasting thermodynamic and kinetic effects, favouring **1α** and **1β**, respectively. Interestingly, during the review of the present article, a very recent publication reported that mechanochemistry resulted in a unique way to expand the crystal landscape of dexamethasone to obtain kinetically stable cocrystals with benzenediols (catechol and resorcinol).⁵²

The **1β** form was experimentally found to be more stable than **1α**, as indicated by TGA and DSC measurements, in contrast to energy framework calculations. DSC also allowed identification of eutectic melting and amorphous solidification in the case of acridine/naproxen mechanical mixtures and cocrystals. Conversely, aminoacridine and naproxen melt separately and then crystallize as a mixture of the reactants with a eutectic solidification. As a final consideration, increasingly substituted acridines are less prone to cocrystallize with naproxen, with acridine showing two molecular cocrystals, 9-aminoacridine showing one molecular cocrystal, and

6,9-diamino-2-ethoxyacridine giving no cocrystals, independently of the adopted preparation procedure.

Conflicts of interest

The authors declare no conflict of interest.

Acknowledgements

The authors acknowledge the Research of Young Scientists grant (BMN) no. 539-T080-B027-22 (University of Gdansk), DS no. 531-T080-D738-22 (University of Gdansk), Project 288-105 by FINPIEMONTE within the Programma Pluriennale Attività Produttive 2015/2017 Misura `3.1 “Contratto d’insediamento” (Università del Piemonte Orientale).

Notes and references

- G. R. Desiraju, Supramolecular synthons in crystal engineering—a new organic synthesis, *Angew. Chem., Int. Ed. Engl.*, 1995, **34**(21), 2311–2327.
- B. Moulton and M. J. Zaworotko, From molecules to crystal engineering: supramolecular isomerism and polymorphism in network solids, *Chem. Rev.*, 2001, **101**(6), 1629–1658.
- G. R. Desiraju, Hydrogen bridges in crystal engineering: interactions without borders, *Acc. Chem. Res.*, 2002, **35**(7), 565–573.
- G. R. Desiraju, Crystal engineering: a holistic view, *Angew. Chem., Int. Ed.*, 2007, **46**(44), 8342–8356.
- N. Shan and M. J. Zaworotko, The role of cocrystals in pharmaceutical science, *Drug Discov. Today*, 2008, **13**(9–10), 440–446.
- D. J. Good and N. Rodriguez-Hornedo, Solubility advantage of pharmaceutical cocrystals, *Cryst. Growth Des.*, 2009, **9**(5), 2252–2264.
- N. K. Duggirala, M. L. Perry, Ö. Almarsson and M. J. Zaworotko, Pharmaceutical cocrystals: Along the path to improved medicines, *Chem. Commun.*, 2016, **52**(4), 640–655.
- A. Port, C. Almansa, R. Enrech, M. Bordas and C. R. Plata-Salamán, Differential Solution Behavior of the New API-API Co-Crystal of Tramadol-Celecoxib (CTC) versus Its Constituents and Their Combination, *Cryst. Growth Des.*, 2019, **19**(6), 3172–3182.
- M. Isidori, M. Lavorgna, A. Nardelli, A. Parrella, L. Previtiera and M. Rubino, Ecotoxicity of naproxen and its phototransformation products, *Sci. Total Environ.*, 2005, **348**(1–3), 93–101.
- P. A. Todd and S. P. Clissold, Naproxen: A Reappraisal of its Pharmacology, and Therapeutic Use in Rheumatic Diseases and Pain States, *Drugs*, 1990, **40**(1), 91–137.
- C. Bombardier, L. Laine, A. Reicin, D. Shapiro, R. Burgos-Vargas, B. Davis, R. Day, M. B. Ferraz, C. J. Hawkey, M. C. Hochberg, T. K. Kvien and T. J. Schnitzer, Comparison of upper gastrointestinal toxicity of rofecoxib and naproxen in patients with rheumatoid arthritis, *N. Engl. J. Med.*, 2000, **343**(21), 1520–1528.



- 39 Johnson, C.K., ORTEP II, Report ORNL-5138, Oak Ridge National Laboratory, Oak Ridge, TN, USA, 1976.
- 40 Motherwell, S.; Clegg, S. PLUTO-78, Program for Drawing and Molecular Structure, University of Cambridge, Cambridge, UK, 1978.
- 41 C. F. Macrae, I. J. Bruno, J. A. Chisholm, P. R. Edgington, P. McCabe, E. Pidcock, L. Rodriguez-Monge, R. Taylor, J. van de Streek and P. A. Wood, Mercury CSD 2.0—New Features for the Visualization and Investigation of Crystal Structures, *J. Appl. Crystallogr.*, 2008, **41**, 466–470.
- 42 A. Altomare, C. Cuocci, C. Giacovazzo, A. Moliterni, R. Rizzi, N. Corriero and A. Falcicchio, EXPO2013: a kit of tools for phasing crystal structures from powder data, *J. Appl. Crystallogr.*, 2013, **46**(4), 1231–1235.
- 43 A. A. Coelho, TOPAS and TOPAS-Academic: an optimization program integrating computer algebra and crystallographic objects written in C++, *J. Appl. Crystallogr.*, 2018, **51**(1), 210–218.
- 44 URL: <https://www.topas-academic.net/>.
- 45 C. F. Mackenzie, P. R. Spackman, D. Jayatilaka and M. A. Spackman, CrystalExplorer model energies and energy frameworks: extension to metal coordination compounds, organic salts, solvates and open-shell systems, *IUCrJ*, 2017, **4**(5), 575–587.
- 46 S. P. Thomas, P. R. Spackman, D. Jayatilaka and M. A. Spackman, Accurate lattice energies for molecular crystals from experimental crystal structures, *J. Chem. Theory Comput.*, 2018, **14**(3), 1614–1623.
- 47 P. Rossi, J. Ceccarelli, S. Milazzo, P. Paoli, J. Morais Missina, S. Ciattini, A. Ienco, G. Tuci, M. Valleri, M. P. Giovannoni, G. Guerrini and L. Conti, Nonsteroidal Anti-Inflammatory Drugs–1-Phenylethylamine Diastereomeric Salts: A Systematic Solid-State Investigation, *Cryst. Growth Des.*, 2021, **21**(12), 6947–6960.
- 48 Y. Kobayashi, K. Kinbara, M. Sato and K. Saigo, Synthesis, absolute configuration, and application of enantiopure trans-1-aminobenz [f] indan-2-ol, *Chirality*, 2005, **17**(2), 108–112.
- 49 J. Bao, Z. Zhang, Z. Yan, J. R. Wang and X. Mei, Cocrystallization in vitamin B9 gels to construct stoichiometry-controlled isostructural materials, *CrystEngComm*, 2018, **20**(12), 1644–1648.
- 50 M. Rajkumar, A non-centrosymmetric cocrystal assembled by OH...N and CH... π supramolecular synthons, *J. Mol. Struct.*, 2021, **1245**, 131105.
- 51 D. K. Bučar, R. W. Lancaster and J. Bernstein, Disappearing polymorphs revisited, *Angew. Chem., Int. Ed.*, 2015, **54**(24), 6972–6993.
- 52 S. N. Wong, K. H. Low, J. Weng, H. W. Chan and S. F. Chow, Expanding the solid-state landscape of dexamethasone: a specific sandwich structure in facilitating the formation of kinetically stable cocrystals from mechanochemistry, *CrystEngComm*, 2022, **24**, 5875–5879.

